Flexible, Transparent, and Noncytotoxic Graphene Electric Field Stimulator for Effective Cerebral Blood Volume Enhancement

Chaejeong Heo,[†,‡] Si Young Lee,[†,‡] Areum Jo,[§] Susie Jung,[§] Minah Suh,[§,⊥,*] and Young Hee Lee[†,‡,*]

[†]IBS Center for Integrated Nanostructure Physics (CINAP), Institute for Basic Science, Daejeon 305-811, Korea, [‡]Department of Physics, Sungkyunkwan Advanced Institute of Nanotechnology, Department of Energy Science, Sungkyunkwan University, Suwon 440-746, Korea, [§]Department of Biological Science, Sungkyunkwan University, Suwon 440-746, Korea, and [⊥]Samsung Advanced Institute for Health Science and Technology, Sungkyunkwan University, Suwon 440-746, Korea

ABSTRACT Enhancing cerebral blood volume (CBV) of a targeted area without causing side effects is a primary strategy for treating cerebral hypoperfusion. Here, we report a new nonpharmaceutical and nonvascular surgical method to increase CBV. A flexible, transparent, and skin-like biocompatible graphene electrical field stimulator was placed directly onto the cortical brain, and a noncontact electric field was applied at a specific local blood vessel. Effective CBV increases in the blood vessels of mouse brains were directly observed from *in vivo* optical recordings of intrinsic signal imaging. The CBV was significantly increased in arteries of the stimulated area, but neither tissue damage nor unnecessary neuronal activation was observed. No transient hypoxia was observed. This technique provides a new method to treat cerebral blood circulation deficiencies at local vessels and can be applied to brain regeneration and rehabilitation.

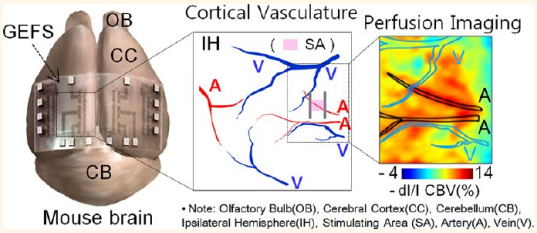

KEYWORDS: graphene · electrical field stimulation · cerebral blood volume · cerebral blood flow · hemodynamics · *in vivo*

The global population is aging; thus, the risk for cerebrovascular diseases and associated deaths is rapidly increasing. One therapeutic strategy for cerebrovascular diseases of hypoperfusion, such as cerebral infarction,[1−3] arteriosclerosis,[4] ischemia,[5] dementia,[1−3,6] and vascular Parkinsonism,[7,8] is to increase the cerebral blood volume (CBV) of the focal area. Prior strategies include injection of anticoagulant,[9,10] stent insertion,[11] and applying direct current stimulation (DCS).[12] DCS can lead to neuronal activation, an increase of cerebral metabolic demands, and will eventually increase CBV.[12,13] Although these methods are useful for increasing CBV, side effects are often observed, including increased risk of secondary bleeding,[14,15] global blood volume increases,[15,16] and safety issues that include unnecessary neural tissue activation and possible tissue damage.[17,18] Especially at high amplitude of current, DCS may disrupt synaptic activity, desynchronization, and neurotransmitter depletion[19,20] and leads into the transient focal ischemia,[21] which can interrupt cortical processing. Here, we propose a new strategy with a skin-like biocompatible stimulator to minimize such side effects and furthermore to apply more effective noncontact electric field (nEF) stimulation. This stimulator is fabricated with an ultrathin electrode of graphene, two-dimensional honeycomb arrangement of carbon atoms which yields superb electrical conductivity, high transmittance, and excellent flexibility.[22−24] We hypothesize that nEF stimulation is an effective way to enhance cerebral perfusion with stronger arterial correlation than DCS, without evoking unnecessary neuronal activation and focal transient hypoxia.

RESULTS

A schematic of the fabrication process of graphene electrical field stimulator (GEFS) is shown in Figure 1A. The fabricated GEFS is a skin-like film with a thickness of 150 ± 50 μm with a biocompatible PDMS cover that avoids direct contact of the

* Address correspondence to leeyoung@skku.edu, minahsuh@skku.edu.

Received for review December 20, 2012 and accepted May 6, 2013.

Published online May 06, 2013
10.1021/nn305884w

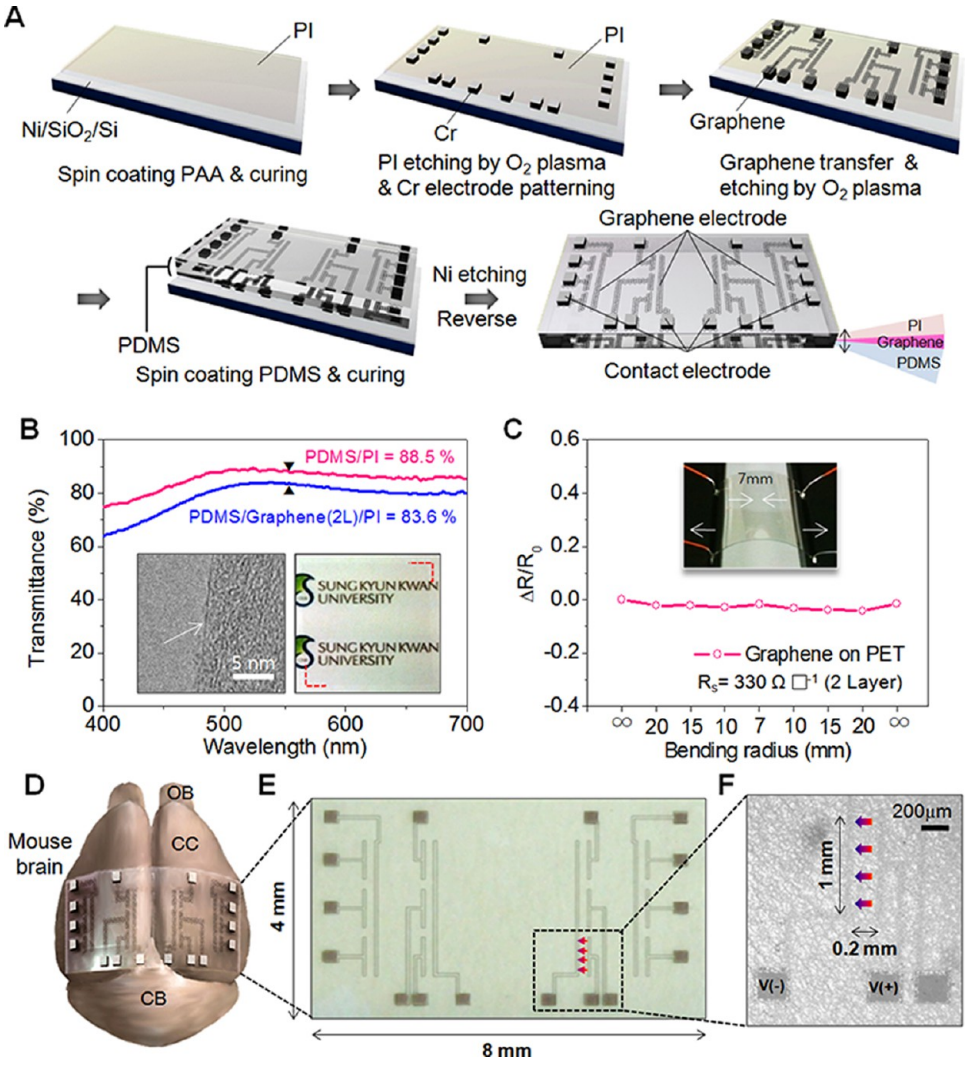

Figure 1. Schematic of the GEFS and physical characteristics of graphene. (A) Thin layer of polyamic acid (PAA) was spin-casted on a Ni (50 nm)/SiO_2/Si substrate and cured to form PI. The squared Cr electrode pattern was formed by combining photolithography with reactive oxygen ion etching. Two layers of graphene were transferred using a layer-by-layer process (see Figure S1, Supporting Information). After patterning the graphene electrode with a similar etching process, PDMS was coated on the patterned graphene layer. The Ni/SiO_2/Si support substrate was then removed by Ni etching. The reversed electrode in the last step shows that the graphene electrodes are squeezed between the top PI and bottom PDMS layers, which are interconnected to the Cr contact electrodes and can be connected to an external power source. (B) Transmittance of GEFS with or without the graphene layer. Values are provided at a wavelength of 550 nm. Monolayer of graphene (arrow) is shown in the transmission electron microscopy (TEM) image (left inset) and demonstrates the optically transparent image (right inset). (C) Resistance variance by bending the graphene (2 layers) placed on the PET film. (D) Illustration of a GEFS-adhered curved mouse brain where contact Cr electrodes are exposed. OB, olfactory bulb; CC, cerebral cortex; CB, cerebellum. (E) Magnified (and slightly modified) electrode image to visualize the graphene electrode pattern. (F) Detailed specification of the graphene electrode, including polarity and direction of electric field, within the dotted box in (E).

graphene with the tissue. The detail fabrication process is shown in Figure S1 (Supporting Information). The transmittance of the GEFS film was 83.6% (88.5%) in the presence (absence) of graphene (Figure 1B), which was in accord with 2.3% absorbance per monolayer of graphene[22] (Figure S2, Supporting Information). High transmittance is a key factor for real-time optical recordings of intrinsic signal (ORIS) imaging of cerebrovascular structures. Bilayer graphene yielded a sheet resistance of 330 ohm/sq.[25] The resistance variance was tested as a function of bending radius (Figure 1C). The change in the sheet resistance was negligible within 4% as the radius of curvature narrowed down to 7 mm, demonstrating superb flexibility of the GEFS. This bending stability allowed us to make proximate contacts on the curved mouse brain (Figure 1D), which is crucial for efficient field stimulation. The GEFS used in the current study has a thickness of about 150 μm, which is good enough to cover relatively flat cortex of the mouse. The thinner stimulator compared to the current stimulator may be useful in future applications for large-size animals such as cat and monkey, whom have more convulsive brain surface curvature than the mouse brain. The patterned electrode is shown with guided

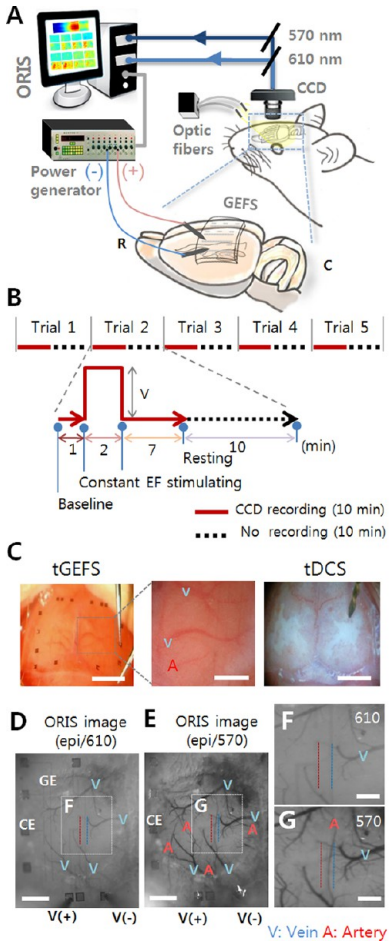

Figure 2. ***In vivo*** **experimental setup for ORIS imaging and the diagram for nEF stimulation. (A) Illustration of the ORIS experimental set up for** ***in vivo*** **cortical imaging. The CCD camera connected to optical filters (570 and 610 nm) takes images of the cortical surface, which are sent to the ORIS recording system. White light is transmitted through two optical fibers to illuminate the cortical surface for ORIS. The mouse brain is covered with GEFS to apply nEF on the specific artery blood vessel. The contact electrode in the GEFS is connected to a power generator. R, rostral; C, caudal. (B) Electric field stimulation paradigm consists of 5 stimulation trials per imaging session. In each trial, the image recording by CCD (red line) lasts for 10 min, which includes a 1 min baseline, 2 min of stimulation, and 7 min of post-stimulation. No recording session followed for 10 min in each trial to ensure the recovery of hemodynamic responses after stimulation. (C) Neurovasculature under tGEFS with transcranial approach (left; scale bar: 2 mm). Veins and arteries are clearly visible in the magnified image (middle; scale bar: 1 mm). A comparative image obtained by tDCS (right; scale bar: 2 mm). GEFS is applied on the cortex with epidural approach and ORIS images of the cortex under the GEFS taken through (D) a 610 nm filter and (E) a 570 nm filter. (F,G) Corresponding magnified areas shown in (D) and (E). In particular, the arteries located within the two graphene electrodes (red and blue) are clearly seen under the 570 nm filter in (G). CE, contact electrode; GE, graphene electrode; V(+), positive input line; V(−), neutral input line. Scale bars in (D,E) = 1 mm; (F,G) = 0.5 mm.**

lines for graphene electrodes (Figure 1E), and the magnified optical image demonstrates an electrode length of 1 mm with a gap of 0.2 mm between electrodes (Figure 1F). The strong local electric field can be applied to the confined region of a cortical blood vessel because of the micrometer-size interdigital electrode. The locally confined electric field allows stimulation of the blood vessel with targeted specificity. As long as no cerebrospinal fluid is overflown into the surface of the electrode, leakage current can be avoided. For better safety, wire leads could be formed from all of the electrodes.

The *in vivo* effect of nEF stimulation on CBV is assessed by ORIS. The GEFS is mounted over the whole brain of an anaesthetised mouse (Figure 2A) and delivered the programmed stimulation (Figure 2B). Figure 2C shows the cortical blood vessels under the skull through the transcranial GEFS (tGEFS) film compared with the transcranial DCS (tDCS) image (for tDCS experiment, see Figure S3, Supporting Information). The tDCS is applied to the cortex *via* a metal electrode placed on the skull. Clear vessel images are shown with tGEFS. GEFS film with high transmittance enables clear ORIS images and prevents the skull from being dehydrated. For the stimulation on the artery closely, the skull was removed by craniectomical surgery and exposed epidural cortex. In ORIS imaging, veins were predominantly visualized with 610 nm filter due to the high sensitivity to the changes in deoxyhemoglobin[21,26] (Figure 2D,F). However, both veins and arteries were visualized with 570 nm filter, anisosbestic wavelength of oxyhemoglobin and deoxyhemoglobin absorption[21,26] (Figure 2E,G). One of the advantages of placing GEFS film on the animal's brain surface is to prevent the brain from swelling and reduce pulsation artifacts and, therefore, to ensure the physiological healthiness of cortical tissue. The electric field formed between these two electrodes stimulates the cortical artery between the two electrodes with opposite polarities (Figure 2D−G). The exact locations of electrodes in relation to the cortical vasculature within our regions of interest (ROI, white dashed squares in Figure 2D,E) are shown in Figure 2F,G.

The changes in CBV induced by nEF stimulation through GEFS are shown in Figure 3. The ORIS signal was analyzed from the stimulating area (SA, red ROI) on the artery of the ipsilateral hemisphere (IH) and from the control area (CA, blue ROI) at the mirror place (on the artery) of the contralateral hemisphere (CH) in Figure 3A. Then EF was applied to the selected area focusing on the artery (Figure 3B). We studied voltage amplitude dependency of the cortical perfusion changes (Figure 3C). The change in the maximum CBV in the SA increased significantly at 0.9 V/mm, while the maximum CBV in the CA was unchanged. As the field strength was increased to 9 V/mm, not only the maximum CBV at the SA but also the maximum CBV at the CA was increased even though the CBV increase of CA was not statistically significant. The nEF stimulation yields significantly larger increases of CBV in the SA

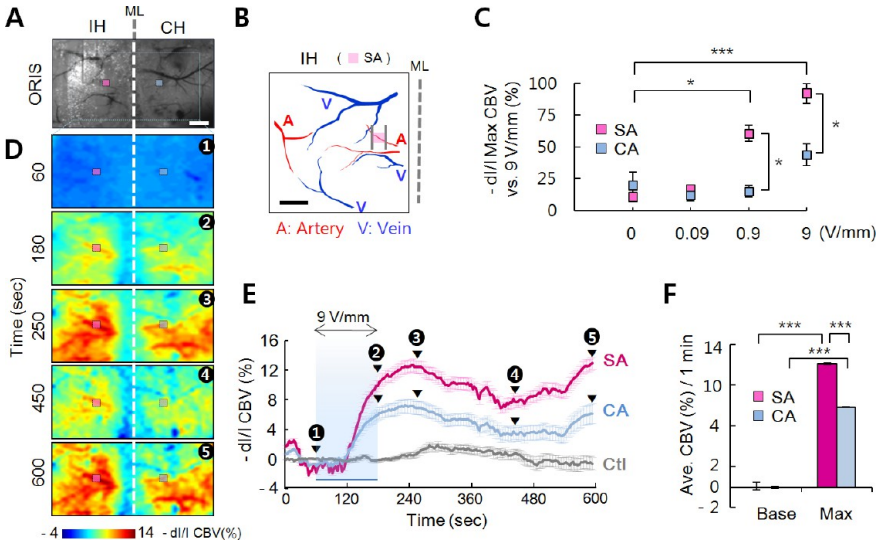

Figure 3. Changes of cortical perfusion induced by nEF stimulation using GEFS. (A) Raw ORIS images of the cortical surface covering with GEFS under a 570 nm optical filter. The cortical surface was divided into the ipsilateral hemisphere (IH) and the contralateral hemisphere (CH). Two ROIs, one from the SA of the IH (red square) and another from the CA of the CH (blue square), are shown. ML is the midline between the IH and CH. Scale bar: 0.5 mm. (B) Illustration of the cortical vasculature of the IH. The electric field is applied to the SA on the artery. Scale bar: 0.5 mm. (C) Maximum CBV values (±SEM) are shown as functions of field strength at SA and CA. The difference becomes more prominent at a field strength >0.9 V/mm; *$p < 0.05$ and ***$p < 0.001$ ($n = 3$ for each group). (D) Typical example of ORIS map of CBV on the cortical surface for 600 s at 9 V/mm, and red (blue) color represents increased (decreased) CBV with scale bar (% of −dI/I CBV). (E) Representative graph for changes in CBV after stimulation for 120 s at SA and CA. The maximum change in CBV appeared at 250 s (number 3) in the SA and was maintained for 10 min with minor fluctuations. A similar pattern was observed in the CA, although the maximum value was lower than that of the SA but clearly distinct from the sham control (Ctl). (F) Average values (±SEM) of the CBV changes for 1 min near the maximum CBV compared with that of the baseline ($n = 12$). Significant changes in CBV in the SA and CA were observed (*$p < 0.001$).**

than those of the CA at 0.9 and 9 V/mm ($n = 3$ for each group) (Figure 3C).

The ORIS map of both hemispheres and the temporal profile of CBV changes of SA and CA under 9 V/mm nEF stimulation are shown in Figure 3D,E. This figure is for a typical example from one animal. The CBV change was stronger in the IH, as shown in Figure 3C. The change in CBV was not appreciable in the initial stage of stimulation but became more prominent and revealed a maximum (~12%) at approximately 250 s (mark 3) in the SA. The increase in CBV was maintained over 600 s with minor fluctuations; the change decreased to 8% at 450 s (mark 4) and increased again to almost 12% at 600 s (mark 5). The consistent CBV increase by nEF stimulation with GEFS contrasted markedly with the results of DCS, which revealed that the increase in CBV disappeared after stimulation (Figure S4A, Supporting Information). A similar profile was also observed in the CA, although the change was less than that in the SA (Figure 3E). Furthermore, these values were clearly distinct from a sham control mouse with no stimulation (Ctl in Figure 3E). In addition, the CBV was dramatically increased both in the SA and CA because of the vasculature connection between two hemispheres, although the changes in CBV of the CA were smaller than those in the SA because the CA was not stimulated with GEFS (Figure 3F, $n = 12$). The nEF stimulation may stimulate deeper brain regions, such as the thalamus, than DCS that stimulates rather superficial cortical layers. Therefore, nEF stimulation may yield stronger and more direct thalamic influences than DCS and cause strong activation of the cortical–thalamic connection leading to higher contralateral hemispheric responses than DCS. In order to further support this, one may conduct the whole brain imaging, such as near-infrared spectroscopic (NIRS) imaging and functional magnetic resonance imaging (fMRI), under the nEF stimulation. These studies may help us to elucidate the possible mechanism of bilateral responses upon nEF stimulation.

To compare the effect of nEF stimulation with DCS, the ORIS map of CBV under DCS is shown in Figure 4A. The CBV in the IH was increased significantly 300 s after stimulation, while the CBV did not change in the CH. The profile of CBV changes at the SA and CA is shown in Figure S4 (Supporting Information).

Spatiotemporal representations of the changes in CBV with nEF stimulation at 9 V/mm over 2 min periods (top panel) and with DCS at 0.1 mA over 15 s periods (bottom panel) are shown in Figure 4B. In order to directly compare CBV change between nEFS and DCS, the maximum CBV was shown at around 10%. This yielded a field strength of 9 V/mm for a duration time of 2 min in GEFS and a current of 0.1 mA for a duration time of 15 s in DCS. In order to select the stimulation parameters for DCS, we have conducted a series of

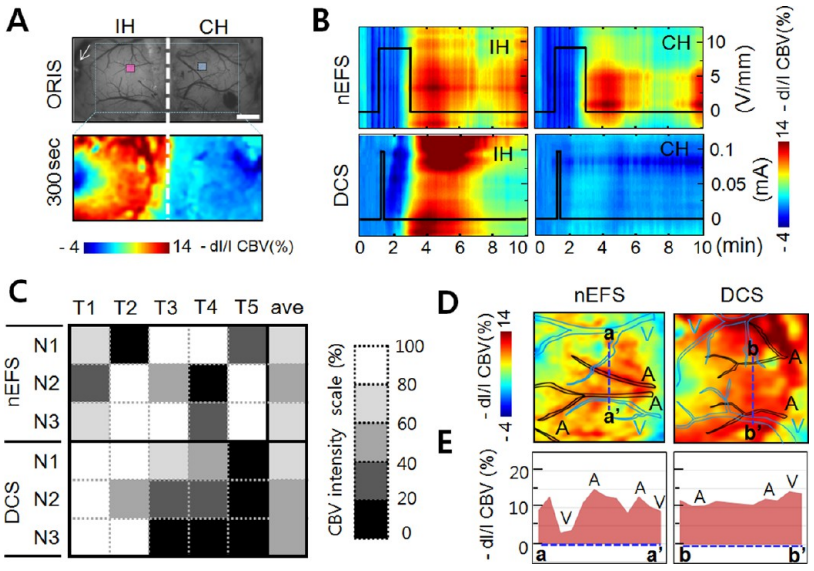

Figure 4. (A) ORIS image (570 nm) and their intensity map at 300 s with DCS. The arrow in the IH indicates the electrode. Scale bar: 0.5 mm. (B) Spatiotemporal representation of changes in the CBV with nEF stimulation at 9 V/mm (top panel) for 2 min and DCS at 0.1 mA (bottom panel) for 15 s. Each figure is created by summing the horizontal pixel value of the images at each vertical pixel point. The changes in CBV were maintained with transient nEF stimulation. (Note: nEFS in the figures indicates nEF stimulation.) (C) Three examples of scaled CBV changes (SA) over 5 trials for each animal following stimulation with the nEFS and DCS. The CBV changes are classified into five categories, with white being the strongest change and black being the weakest. In each animal (N1, N2, N3), the change in CBV at each trial was examined and quantified. The "ave" is the average CBV changes for 5 trials (T1−T5). (D) Blood vessel distribution and the changes in CBV of the IH with nEF stimulation and DCS. The nEF stimulation caused vasculature-specific changes in the CBV, while DCS is nonspecific. (E) Intensity profile for each dashed line (a-a′, b-b′) in (D). The intensity changes with the positions of arterial vessels with nEF stimulation, while no vessel-specific pattern was observed with DCS.

DCS experiments with varying amplitude and duration (Figure S5, Supporting Information). A consistent change in CBV was clearly seen with nEF stimulation in both the IH and CH after stimulation. However, transient changes in CBV were only seen in the IH with DCS. The transient decrease of the CBV was also observed right after DCS (Figure S4A, Supporting Information) due to immediate neuronal activation following DCS. Interestingly, the average increase in CBV for 5 trials of stimulation was well manifested with nEFS, and the increases in CBV were reproducible after breaks for 5 trials, with low interindividual variability (Figure 4C). This was in contrast with DCS, in which the increase in CBV was observed mostly in the initial trial (Figure 4C). Significant CBV changes are observed in the nEFS regardless of the sequence of the trial, that is, large CBV changes (80−100% increase) compared with changes from no stimulation, even in the last trial. However, the changes in CBV with DCS were significant in the first trial but not in the last trial. The average changes in CBV over the 5 trials following the nEFS and DCS are similar, ranging from 10 to 15% higher than the baseline CBV. The nEFS produces more persistent and reproducible changes in CBV compared with DCS. The more cases were showed in Figure S6 (Supporting Information).

To study the vasculature correlating effects of nEF stimulation, cortical blood vessel and the ORIS map of CBV intensity were merged (Figure 4D). The pattern of CBV intensity coincides with the positions of arteries in SA with nEF stimulation, and the heightened CBV by nEF stimulation is better correlated with arterial vasculature, while no vessel-specific pattern was observed with DCS (Figure 4D,E). The DCS elicits non-vessel-specific CBV increase in both veins and arteries, probably due to strong neuronal activation in the SA (Figure 5I,J). Also, we calculated the spatial extents of CBV changes under nEF stimulation and DCS (Figure S7, Supporting Information). The spatial extent of CBV following nEF stimulation is quite focal within the patterned electrodes and resembles arterial vasculature, while the spatial extent following DCS is rather broad and occupies almost the whole cortical area. Thus, this spatial extent data also supports that nEF stimulation causes CBV changes that are highly correlated with vasculature.

Utilizing a probe-type LDF, we measured and compared the CBF changes under nEF stimulation as well as DCS. The LDF experimental schematic, including the measurement locations, is shown in Figure 5A. The nEF stimulation induces strong CBF changes for both 9 V/mm (7.3 ± 1.8%, $n = 7$) and 90 V/mm (13.7 ± 2.8%, $n = 5$) stimulations (Figure 5B), while DCS yields a decrease in CBF (−18.6 ± 15.6%, $n = 2$) at LDF measuring site during the 2 min stimulation period (Figure 5C−F). These data suggest that nEF stimulation is a more effective way to yield CBF increase than DCS.

The local field potential (LFP) recording of pre-, during, and post-DCS exhibits clearly different firing patterns (Figure 5H,I). Slow delta (1−4 Hz) rhythms,

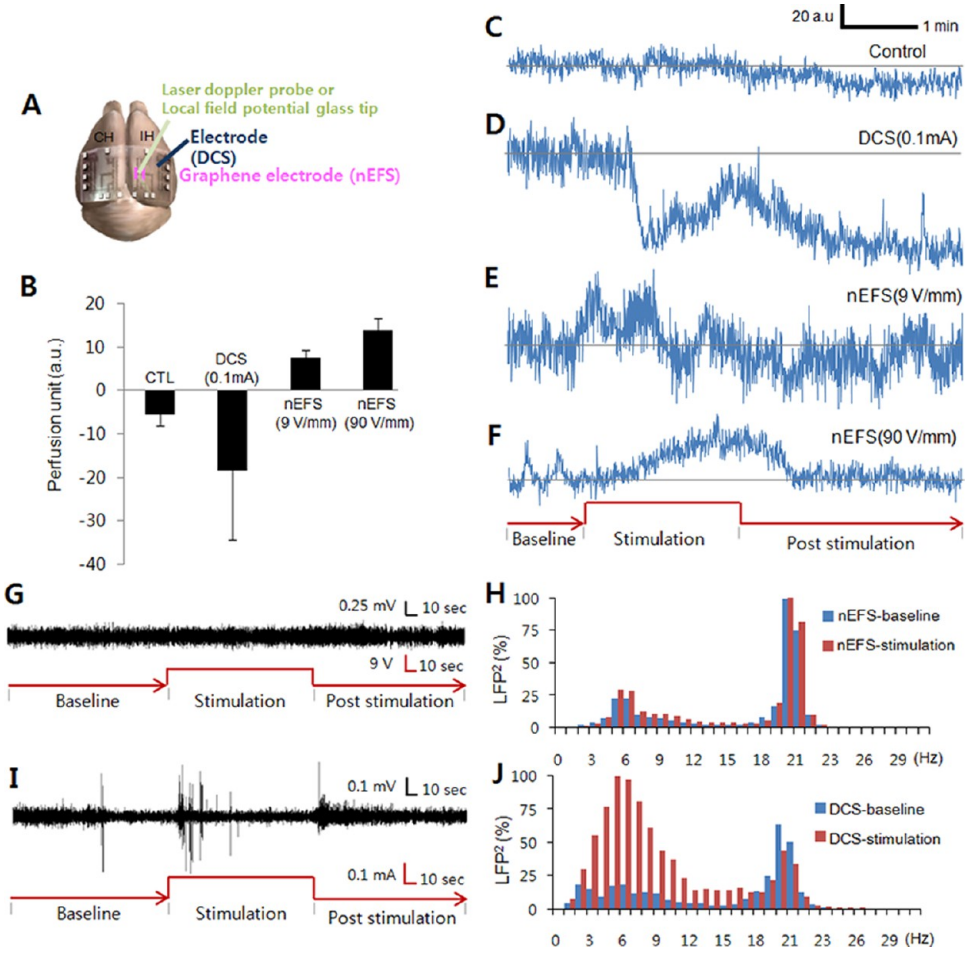

Figure 5. Laser Doppler flowmetry monitoring (C−F) and local field potential (G−J) under the stimulation. (A) LDF and LFP measurement location and schematic. (B) Average changes of CBF (±SEM) during stimulation (2 min) *versus* baseline (1 min). LDF monitoring for control (C), DCS stimulation (D), and nEF stimulation (9 V/mm (E), 90 V/mm (F)). (G,I) Examples of LFP recodings in SA following nEFS and DCS, respectively. (H,J) Comparisons of neural firing frequency patterns following nEFS and DCS.

theta (5−7 Hz) rhythms, and spindle-like (7−15 Hz) waveform of LFP become more prominent during DCS than the baseline, indicating increased arousal and synchronous thalamic-cortical neuronal firing due to DCS (Figure 5I).[27] In contrast, nEF stimulation seems to selectively stimulate the arteries in the targeted area without provoking any unnecessary neuronal activation (Figure 5G). No differences were found in firing patterns of LFP pre-, during, and post-nEF stimulation (Figure 5G,I). The frequency analysis of LFP recording suggests that nEF stimulation did not bring any changes in the beta (20−30 Hz) rhythm dominated waveform, a common waveform during rapid eye movement (REM) sleep and waking state without conducting specific tasks (Figure 5H).

Thus, our developed graphene electrode delivers nEF stimulation into the brain tissue but causes no apparent neuronal excitation, and thereby led to no clear focal hypoxia during the stimulation. Conventional DCS causes large changes in CBV but more strongly affects neuronal population than nEF; therefore, DCS brings about strong neuronal excitation and subsequent decreases in CBV, such as hypoxic response. These results are supported by both CBV measurements by intrinsic signal optical imaging and CBF measurements by LDF.[31]

However, both of our LFP and LDF recordings are from superficial cortical layers, and we may not be able to directly record neuronal activation and hemodynamics of deep brain regions. The nEF stimulation may stimulate deeper brain region and yield stronger and more direct thalamic influences than DCS, which will cause strong activation of cortical thalamic connection, therefore higher contralateral hemispheric responses.

Immunohistochemistry was also performed to assess the effect of nEF stimulation and DCS on brain (Figure 6). The overall brain morphology is shown in Figure 6A−F. Figure 6G−I,L shows H&E staining. The brain tissue well preserved the morphological features (Figure 6A,D,G) with 2 min nEFS, while some blood was found on the stimulated cortex with 2 min DCS (Figure 6E,L). Neither apparent cell damage nor death was observed in the CA or SA with nEFS (Figure 6H,I).

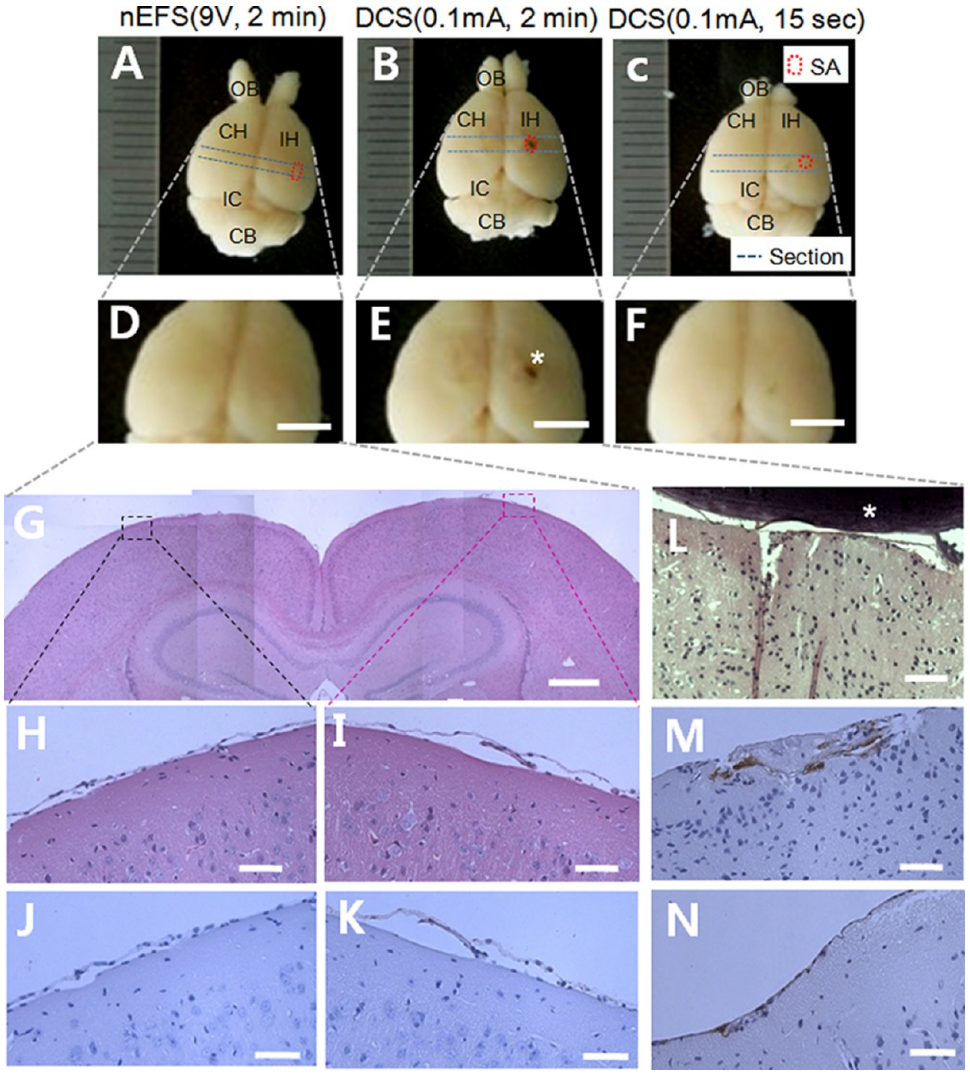

Figure 6. Immunohistological analysis of nEFS and DCS. The brain was extracted after 5 rounds of stimulation; blue lines indicate sectioning in the coronal plane. The SA (red area) is in the primary sensory cortex in the IH and magnified images of surface in the cortex with nEF (D) and DCS (E,F). OB, olfactory bulb; IC, inferior colliculus; CB, cerebellum. (G,L) H&E stained images of the sectioned cerebral cortex of nEFS (G) and of DCS (L) with same stimulation duration (2 min). Scale bar: (G) 1 mm and (L) 250 μm. The black square (CA) in the CH and the red square (SA) in the IH are magnified in (H) and (I), respectively. Comparison image of TUNEL staining of CA and SA with 2 min nEFS (J,K) and 2 min DCS (M) and with 15 s DCS (N). The brown staining indicates a dead cell. Tissue damage was not observed in the brain tissue with nEFS (J,K), while some brown dead cells were observed in the brain tissue with DCS (M,N). (E,L) Asterisk * marked of blood clot in cortex. Scale bars: (H−M) 250 μm.

This was confirmed by TUNEL staining (Figure 6J,K). The epidural DCS lasting 2 min caused cortical damage (Figure 6E,L) and showed positive dead cells in TUNEL staining in SA (M,N). The DCS lasted for 15 s and yielded some tissue damage and dead cells. Thus, the tissue damage became more severe when the DCS was prolonged for 2 min. The cytotoxicity under nEF stimulation has also been investigated in our previous neuronal cellular study *in vitro*, which did not show any morphological deformation or apoptosis in neural cells.[24]

DISCUSSION

Direct cortical stimulation has been applied *in vivo* for clinical mapping[28] and is related to the direct depolarization of cell somata and axons.[29] Direct electrical stimulation, especially at high amplitudes of current, may disrupt synaptic activity and produce desynchronization and neurotransmitter depletion,[30,31] which leads to a transient focal ischemia with a 1 cm^2 area[31] and interrupts cortical processing. The noncontact electric field stimulation using graphene electrodes in the current study confined the activated area between the graphene negative and positive electrodes, which were approximately 0.2 mm^2 (see Figure 3, vessel activation). We hypothesized that nEF would more effectively enhance cerebral perfusion without disrupting cortical processing and focal hypoxia. We also hypothesized that the nEF stimulation would neither directly depolarize cell somata and axons[29] nor disrupt synaptic activity and neurotransmitter depletion.[30,31] We recorded LFP within the stimulated area under nEF stimulation through the

graphene stimulator or direct electric current stimulation using conventional electrodes to investigate this hypothesis (Figure 5G–J). No significant neuronal activation was observed using nEF stimulation, but strong neuronal activation was observed using DCS. Therefore, nEF stimulation ensured normal cortical processing without potential disruption and with enhanced CBV and CBF. However, further research should be performed to delineate the exact physiological mechanisms of nEF stimulation using graphene electrodes.

The developed graphene neural stimulator has few limitations for the clinical application. One limitation is that the current form of stimulator can be applied over the surface of the brain. Further modification of the developed graphene stimulator to accommodate deep brain structure or for use over the intact skull should be incorporated. Such modification could include a combination approach with the catheterization.[11]

CONCLUSIONS

Our nEF stimulation using GEFS exhibits several advantages over typical DCS using metal electrodes. First, the GEFS system is flexible and offers superb visibility for ORIS imaging due to its transparency. Second, nEF stimulation elicits robust CBV changes in the IH and CH of the cortex, and these changes in CBV are strongly correlated with the arterial vasculature of the cortex. In contrast, DCS elicits strong but nonspecific changes in CBV exclusively in the IH. Third, the effect of nEF stimulation is prolonged, while the effect of DCS is transient. In other words, nEF stimulation generates stable hemodynamic modulation. Lastly, nEF stimulation is safer than DCS. No obvious tissue or cellular damage was observed following nEF stimulation. No transient decease in CBV and CBF was also observed. In addition, the immediate blood flow increase with nEF stimulation is not likely due to direct strong activation of neurons, and therefore, it can ensure cortical processing without possible disruption. Thus, our results suggest that nEF stimulation with a GEFS may be developed as an alternative therapeutic approach for cerebrovascular diseases with perfusion deficits if one can systematically study the physiological mechanism of nEF stimulation.

MATERIALS AND METHODS

Fabrication of the Stimulator. We fabricated the *in vivo* electric field stimulator using a graphene patterned electrode, which was created by insertion between the PI and PDMS, as shown in Figure 1A. The detailed procedure is described in Supporting Information Methods.

Animal and Surgical Experiments. All animal experiments were conducted in accordance with the ethical guidelines of the Institutional Animal Care and Use Committee of Sungkyunkwan University. The mice (strain: CD1, male) were purchased from Orient Bio (ORIENT BIO Inc., Seongnam, South Korea). All mice were housed in a specific pathogen-free (SPF) facility with 60% humidity at 23 °C under a 12 h light/dark cycle and were fed food and water ad libitum. For the experiment, we used 10 week old mice and weighed each mouse (average weight = 35–40 g) before the procedure. The mice were positioned in the stereotaxic apparatus (David Kopf Instruments, CA, USA) and anaesthetised with 1–3% isoflurane (BK Pham, Goyang, South Korea) initially and maintained with 1.5% isoflurane through the respiratory system and then were prepared for surgery. The skull covering the right and left cortical hemispheres from bregma to lambda was removed with a craniotomy using a dental drill (MICROTORQUE II, NJ, USA), and the epi-dura was exposed. After the surgery, we covered the intact dura mater of the curved hemispheres with the graphene stimulator. During experiments, heart rate (250–300 beat/min), arterial pulse (80–100 mmHg), and saturation percentage of O_2 (SpO_2; >85%) were monitored by pulse oximeter (Med Associates Inc., VT, USA). After the experiment, the brain was extracted surgically in a clean hood, fixed with 4% paraformaldehyde, and stored at 4 °C.

Optical Recording Intrinsic Signal (ORIS) Imaging. The ORIS imaging was obtained by the Optical Imager 3001 system (Optical-Imaging, Inc., Jerusalem, Israel), and the exposed epi-dural cortex covered by the GEFS was illuminated with two optic fibers through a halogen lamp illuminator. Reflected light was collected by tandem lenses and was filtered with 570 or 610 nm band-pass filters depending on the oxygenation state of the hemoglobin absorption spectra. An isosbestic wavelength of 570 nm is sensitive to both oxygenated and deoxygenated hemoglobin absorption, and 610 nm is sensitive to the deoxygenated hemoglobin absorption.[21,26] The cerebral blood volume (CBV) change is measured by the total hemoglobin absorption with the 570 nm band-pass filter. The focal plane of the image was 500 μm below the cortical surface with a CCD camera (Adimec-1000m, Adimec, Eindhoven, Netherlands), and the images were acquired with 1000 frames for 10 min of recording. The time from 0 to 1 min before the stimulation was designated as the baseline, and values from 1 to 10 min were divided by this baseline for normalization. All experimental events, such as the electrical stimulation and ORIS, were digitized by Power 1401 (CED, Cambridge, UK) and were recorded with the Spike-2 software system (CED, Cambridge, UK).

Direct Current Stimulation (DCS). After exposing the epi-dura of the mouse brain, a bipolar (2-channel) electrode (Plastics One, Roanoke, VA, USA) was placed in the subregion of the primary somatosensory cortex. The electrode tip was located 1.5 mm caudally from the bregma, approximately 3.0 mm laterally from the midline at an angle ranging from 45 to 60°. The experimental setting for DCS is shown in Figure S3 (Supporting Information). The electrode was connected *via* 2 stimulus isolators (ISO-Flex, A.M.P.I., Jerusalem, Israel) that are controlled by a programmable power generator (Master-8, A.M.P.I., Jerusalem, Israel). All experiments had two main parts, ORIS imaging and inter-recording (no recording), and each experiment was repeated five times. ORIS and inter-recording were performed with 10 min breaks between. ORIS imaging was composed of three parts: pre-stimulation (base recording), stimulation, and post-stimulation (resting or response recording). For all trials, pre-stimulation included CCD recordings for 1 min before stimulation. Stimulation was performed for 15 s at 0.1 mA, and cortical hemodynamic changes were recorded with ORIS imaging. The DCS stimulation parameters were selected after conducting a series of DCS experiments with varying amplitude and duration (0.01 and 0.03 mA; $n = 3$, 0.1 mA; $n = 4$, 1 mA; $n = 5$) (Figure S5, Supporting Information). As a result, we selected DCS parameters that could bring similar CBV changes (within 10% variation ranges of nEF stim responses) with nEF stimulation of the selected parameters.

Noncontact Electric Field Stimulation (nEFS). The graphene stimulator was placed on the epi-dura of the mouse brain (Figure 2A). Two graphene electrodes were chosen for generation of the EF (Figure 1E,F) and were positioned on a specific blood vessel in the cortex. Two Cr contact electrodes extending from the patterning graphene electrodes for generating the

EF (Figure 1F) were connected by +/− wire with contacting electrodes (Figure 2A,C). The contacting electrodes delivered the +/− voltage using an 8-channel programmable power stimulator (Master-8, A.M.P.I., Jerusalem, Israel) and were controlled by two stimulus isolators (ISO-Flex, A.M.P.I. Jerusalem, Israel). A constant electric field was applied to the GEFS for 2 min with the voltage strength of 0.09 mV/mm to 9 V/mm. The stimulation was delivered 5 times for each mouse with optical recording for 10 min followed by a 10 min break and stimulation with nonoptical recording.

Immunohistochemistry and Microscopy. After delivering 5 rounds of nEF or DCS stimulation, the whole brain extracted carefully by microsurgical procedure after the perfusion of mouse with isotonic sodium chloride solution (Dae-Han Pharmaceutical Co. Ltd., Ansan, South Korea) and 4% paraformaldehyde (PFA) solution (Biosesang, Seongnam, South Korea). The brain was fixed with 4% PFA and then sectioned by acryotome to 20 μm thick slices and were mounted onto slides with mounting medium (Dako, CA, USA). The brain tissues were stained with hematoxylin and eosin (H&E) or were subjected to a terminal deoxynucleotidyl transferase dUTP nick end-labeling (TUNEL) assay (*in situ* cell death detection kit; TMR Red; Roche Diagnostics GmbH, Mannheim, Germany). We examined the slides with a fluorescence microscope (AF6000B, Leica Microsystems GmbH, Wetzlar, Germany) at a wavelength of 688 nm or using bright-field microscopy.

Cerebral Blood Volume (CBV) Data Analysis. We used a modified form of the Beer−Lambert law for calculating the CBV and oxygenation of hemoglobin from recorded images in the 570 and 610 nm band-pass filters, respectively. One minute before the stimulation was designated as the baseline phase, and the images recorded after the stimulation were divided by this baseline for signal normalization. We set the area of the applied electric field as the region of interest (ROI; 2 × 2 pixels, one pixel: 100 × 100 μm^2) and compared it with other nonstimulated areas for 10 min. We chose only trials that showed significant changes in CBV between baseline and stimulation for further analysis. Additionally, we investigated the changes in the CBV in the arterial blood vessel connected with the ROI and in the vertically surrounding tissue. To compare spatiotemporal changes for 10 min, we created time-series images in each whole hemisphere (strip image display in Figure 3H). Each pixel (size: 28 × 28 μm^2) value in the vertical line (91 points) was obtained by summing horizontal pixel values of intensity in Figure 3D with nEF stimulation and Figure 3G with DCS. All data were analyzed using custom-written Matlab software (The Mathworks, MA, USA).

Laser Doppler Flowmetry (LDF). CBF was continuously recorded by the PeriFlux System 5000 (wavelength 780 nm, Perimed, Sweden) simultaneously during the stimulation.[31] A small probe-type straight LDF was placed on the GEFS and positioned at the artery within the stimulation area. We measured LDF changes with and without nEF stimulation. For the DCS experiment, the probe-type LDF was kept at the same position as GEFS. We inserted the DCS electrode onto the sensory cortical area through a slit at the GEFS film. A detailed experimental scheme is provided in Figure 5A. LDF data were acquired at 33 Hz with a 0.03 s time constant. We analyzed and displayed the data after binning.

Local Field Potential (LFP) Recording and Analysis. LFP was recorded from the SA using standard electrophysiological recording setting. The glass pipet filled with 0.9% saline was inserted into the cortical layer 2−3 and was connected to an amplifier A-M Systems (World Precision Instruments) and the CED Power 1401/Spike 2 system (Cambridge Electronic Design) for amplification, filtering and fast Fourier transformation (FFT) analysis of LFP. FFT allows frequency analysis of neural firing of pre- and post-stimulation. The experiments were performed 2 animals for control (not shown data) and more than 3 animals for each nEFS (3 trials) and DCS (2 or 3 trials) experiment.

Conflict of Interest: The authors declare no competing financial interest.

Acknowledgment. This work was supported by the Research Center Program of IBS (Institute for Basic Science) and WCU program (R31-2008-10029) of the National Research Foundation of Korea (NRF) grant funded by the Korea government (MEST), and also by a grant of the Korean Health Technology R&D Project, Ministry of Health & Welfare, Republic of Korea (A110097).

Supporting Information Available: Additional experimental details and figures. This material is available free of charge *via* the Internet at http://pubs.acs.org.

REFERENCES AND NOTES

1. Snowdon, D. A.; Greiner, L. H.; Mortimer, J. A.; Riley, K. P.; Greiner, P. A.; Markesbery, W. R. Brain Infarction and the Clinical Expression of Alzheimer Disease. The Nun Study. *JAMA* **1997**, *277*, 813–817.
2. Vermeer, S. E.; Prins, N. D.; den Heijer, T.; Hofman, A.; Koudstaal, P. J.; Breteler, M. M. Silent Brain Infarcts and the Risk of Dementia and Cognitive Decline. *N. Engl. J. Med.* **2003**, *348*, 1215–1222.
3. Schneider, J. A.; Wilson, R. S.; Bienias, J. L.; Evans, D. A.; Bennett, D. A. Cerebral Infarctions and the Likelihood of Dementia from Alzheimer Disease Pathology. *Neurology* **2004**, *62*, 1148–1155.
4. Yamauchi, H.; Nishii, R.; Higashi, T.; Kagawa, S.; Fukuyama, H. Silent Cortical Neuronal Damage in Atherosclerotic Disease of the Major Cerebral Arteries. *J. Cereb. Blood Flow Metab.* **2011**, *31*, 953–961.
5. Dreier, J. P. The Role of Spreading Depression, Spreading Depolarization and Spreading Ischemia in Neurological Disease. *Nat. Med.* **2011**, *17*, 439–447.
6. Zlokovic, B. V. Neurovascular Pathways to Neurodegeneration in Alzheimer's Disease and Other Disorders. *Nat. Rev. Neurosci.* **2011**, *12*, 723–738.
7. Sibon, I.; Fenelon, G.; Quinn, N. P.; Tison, F. Vascular Parkinsonism. *J. Neurol.* **2004**, *251*, 513–524.
8. Nanhoe-Mahabier, W.; de Laat, K. F.; Visser, J. E.; Zijlmans, J.; de Leeuw, F. E.; Bloem, B. R. Parkinson Disease and Comorbid Cerebrovascular Disease. *Nat. Rev. Neurol.* **2009**, *5*, 533–541.
9. Rothwell, P. M.; Algra, A.; Amarenco, P. Medical Treatment in Acute and Long-Term Secondary Prevention after Transient Ischaemic Attack and Ischaemic Stroke. *Lancet* **2011**, *377*, 1681–1692.
10. Kalyanasundaram, A.; Lincoff, A. M. Managing Adverse Effects and Drug−Drug Interactions of Antiplatelet Agents. *Nat. Rev. Cardiol.* **2011**, *8*, 592–600.
11. Nussbaum, E. S.; Mocco, J. *Cerebral Revascularization: Microsurgical and Endovascular Techniques*; Thieme Medical Publishers: Stuttgart, 2011.
12. Zheng, X.; Alsop, D. C.; Schlaug, G. Effects of Transcranial Direct Current Stimulation (tDCS) on Human Regional Cerebral Blood Flow. *Neuroimage* **2011**, *58*, 26–33.
13. Paquette, C.; Sidel, M.; Radinska, B. A.; Soucy, J. P.; Thiel, A. Bilateral Transcranial Direct Current Stimulation Modulates Activation-Induced Regional Blood Flow Changes during Voluntary Movement. *J. Cereb. Blood Flow Metab.* **2011**, *31*, 2086–2095.
14. Warden, B. A.; Willman, A. M.; Williams, C. D. Antithrombotics for Secondary Prevention of Noncardioembolic Ischaemic Stroke. *Nat. Rev. Neurol.* **2012**, *8*, 223–235.
15. Denas, G.; Pengo, V. Current Anticoagulant Safety. *Expert Opin. Drug Saf.* **2012**, *11*, 401–413.
16. Sidtis, J. J.; Tagliati, M.; Alterman, R.; Sidtis, D.; Dhawan, V.; Eidelberg, D. Therapeutic High-Frequency Stimulation of the Subthalamic Nucleus in Parkinson's Disease Produces Global Increases in Cerebral Blood Flow. *J. Cereb. Blood Flow Metab.* **2012**, *32*, 41–49.
17. Agnew, W. F.; McCreery, D. B. Considerations for Safety in the Use of Extracranial Stimulation for Motor Evoked Potentials. *Neurosurgery* **1987**, *20*, 143–147.
18. Nitsche, M. A.; Liebetanz, D.; Lang, N.; Antal, A.; Tergau, F.; Paulus, W. Safety Criteria for Transcranial Direct Current Stimulation (tDCS) in Humans. *Clin. Neurophysiol.* **2003**, *114*, 2220–2222.

19. Nathan, S. S.; Sinha, S. R.; Gordon, B.; Lesser, R. P.; Thakor, N. V. Determination of Current Density Distributions Generated by Electrical Stimulation of the Human Cerebral Cortex. *Electroencephalogr. Clin. Neurophysiol.* **1993**, *86*, 183–192.
20. Haycock, J. W.; Levy, W. B.; Cotman, C. W. Stimulation-Dependent Depression of Neurotransmitter Release in Brain: [Ca^{2+}] Dependence. *Brain Res.* **1978**, *155*, 192–195.
21. Suh, M.; Bahar, S.; Mehta, A. D.; Schwartz, T. H. Blood Volume and Hemoglobin Oxygenation Response Following Electrical Stimulation of Human Cortex. *Neuroimage* **2006**, *31*, 66–75.
22. Nair, R. R.; Blake, P.; Grigorenko, A. N.; Novoselov, K. S.; Booth, T. J.; Stauber, T.; Peres, N. M.; Geim, A. K. Fine Structure Constant Defines Visual Transparency of Graphene. *Science* **2008**, *320*, 1308.
23. Geim, A. K.; Novoselov, K. S. The Rise of Graphene. *Nat. Mater.* **2007**, *6*, 183–191.
24. Heo, C.; Yoo, J.; Lee, S.; Jo, A.; Jung, S.; Yoo, H.; Lee, Y. H.; Suh, M. The Control of Neural Cell-to-Cell Interactions through Non-contact Electrical Field Stimulation Using Graphene Electrodes. *Biomaterials* **2011**, *32*, 19–27.
25. Kim, U. J.; Lee, I. H.; Bae, J. J.; Lee, S.; Han, G. H.; Chae, S. J.; Gunes, F.; Choi, J. H.; Baik, C. W.; Kim, S. I.; *et al.* Graphene/Carbon Nanotube Hybrid-Based Transparent 2D Optical Array. *Adv. Mater.* **2011**, *23*, 3809–3814.
26. Frostig, R. D.; Lieke, E. E.; Ts'o, D. Y.; Grinvald, A. Cortical Functional Architecture and Local Coupling between Neuronal Activity and the Microcirculation Revealed by *In Vivo* High-Resolution Optical Imaging of Intrinsic Signals. *Proc. Natl. Acad. Sci. U.S.A.* **1990**, *87*, 6082–6086.
27. Steriade, M. Grouping of Brain Rhythms in Corticothalamic Systems. *Neuroscience* **2006**, *137*, 1087–1106.
28. Ojemann, G. A. Cortical Organization of Language. *J. Neurosci.* **1991**, *11*, 2281–2287.
29. Ranck, J. B., Jr. Which Elements Are Excited in Electrical Stimulation of Mammalian Central Nervous System: A Review. *Brain Res.* **1975**, *98*, 417–440.
30. Sheth, S. A.; Nemoto, M.; Guiou, M.; Walker, M.; Pouratian, N.; Hageman, N.; Toga, A. W. Columnar sSpecificity of Microvascular Oxygenation and Volume Responses: Implications for Functional Brain Mapping. *J. Neurosci.* **2004**, *24*, 634–641.
31. Zhao, M.; Ma, H.; Suh, M.; Schwartz, T. H. Spatiotemporal Dynamics of Perfusion and Oximetry during Ictal Discharges in the Rat Neocortex. *J. Neurosci.* **2009**, *29*, 2814–2823.